ACS Photonics

Article

pubs.acs.org/journal/apchd5

Omnidirectional Near-Unity Absorption in an Ultrathin Planar Semiconductor Layer on a Metal Substrate

Junghyun Park,[†] Ju-Hyung Kang,[†] Alok P. Vasudev,[†] David T. Schoen,[†] Hwi Kim,[‡] Erez Hasman,[§] and Mark L. Brongersma*[,†]

[†]Geballe Laboratory for Advanced Materials, Stanford University, Stanford, California 94305, United States

[‡]Department of Electronics and Information Engineering, College of Science and Technology, Korea University, Sejong Campus, Sejong-ro 2511, Sejong 339-700, Republic of Korea

[§]Micro and Nanooptics Laboratory, Faculty of Mechanical Engineering and Russell Berrie Nanotechnology Institute, Technion-Israel Institute of Technology, Haifa 32000, Israel

ABSTRACT: We present omnidirectional near-unity absorption of light in an ultrathin planar semiconductor layer on a metal substrate. Using full-field simulations and a modal analysis, it is shown that more than 98% of the incident light energy can be absorbed in a mere 12 nm thick Ge layer on a Ag substrate at the wavelength of 625 nm over a wide range of angles (80% absorption up to 66° in the transverse magnetic and 67° in the transverse electric polarizations). The physical origin of such remarkable absorption properties is the coupling of incident light to the Brewster mode supported by the structure. The modal dispersion connects several critical coupling points in a dispersion diagram at which the absorption is unity and exhibits a virtually flat dispersion relation for both polarizations, resulting in omnidirectional, near-unity absorption. Potential applications of this simple, planar geometry such as photodetectors and solar cells made from various semiconductor materials are also discussed along with feasible charge-extracting structures and performance estimates.

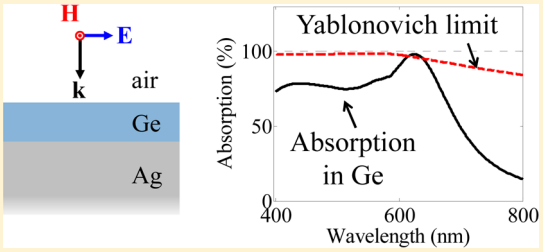

KEYWORDS: *optical absorption, perfect absorber, semiconductor, surface plasmon polariton, critical coupling*

Highly efficient optical absorbers are of critical importance in numerous optical applications such as ultrafast detectors, thermal detectors, and solar cells. The desired features of good optical absorbers include being either robust or sensitive to the wavelength or the illumination conditions such as the incident angle and the polarization state. To realize these features, there has been considerable research on efficient optical absorbers.[1−4] Near-unity absorption for a wide range of incident angles up to 40° was demonstrated by using the localized optical excitation in a nanostructured metal surface.[1] Spectrally selective wide-angle plasmonic absorbers were presented that exploit the localized surface plasmon excitations of metallic nanostructure arrays arranged above a metal reflector with a dielectric spacer.[2−4] Broadband infrared optical absorption was also reported by manipulating the effective conductivity of a metallic film with subwavelength structures.[5] The optical absorbers introduced above are based on one- or two-dimensional nanopatterns and achieve their desirable absorption properties by capitalizing on localized surface plasmons, a modified Fabry−Pérot resonance using effective medium theory, or grating-diffracted waveguide coupling. As a result, these configurations are inevitably accompanied by complex interactions between the multiple resonant modes supported by these geometries. In addition, the fabrication of such two-dimensional nanopatterns of metal pads, disks, coaxial grooves, and other geometries requires an unavoidable increase in the production cost.

For optoelectronic device applications, such as solar cells, photoelectrochemical cells, photodetectors, and modulators, it is highly desirable to facilitate near-unity light absorption in ultrathin, planar semiconductor layers. This could lead to significant performance enhancements and a reduction in materials and processing costs. This realization has prompted considerable research activity toward the design of efficient optical absorbers in stratified media without any applied nanopatterns or texturing. Given the translational invariance in such systems, there is a well-defined single-mode channel that can be excited at a certain frequency and angle of incidence. A typical drawback of these systems tends to be a strong dependence of the absorption on the illumination wavelength and incidence angle. The challenge with the low angle-sensitivity was addressed previously by creating an omnidirectional resonance in a planar metal−dielectric−metal configuration.[6] In this work, it was shown that a Fabry−Pérot-type resonance condition could remain satisfied for a wide range of incident angles due to compensation between the reflection and propagation phases in the cavity. A broadband omnidirectional perfect absorber with an average absorption of 99.3% over the visible regime was demonstrated by sandwiching a Cr film between impedance matching layers on top of a metal mirror.[7]

Received: March 26, 2014
Published: August 1, 2014

Recently, it was also reported that an ultrathin semiconductor layer on top of a noble metal substrate exhibits strongly enhanced optical absorption (up to 70%) in the active material for a wide range of illumination angles.[8] This configuration has provided significant benefits to photoelectrochemical cells based on photoelectrodes that exhibit poor charge transport.[9] However, it still remains a challenge to answer the questions of how to achieve near-unity omnidirectional absorption in an ultrathin, deep subwavelength, planar semiconductor layer and how such strong absorption would be related to the optical modes supported by such a system.

In this paper, we investigate optical absorption properties in a simple planar three-layer system composed of air/semiconductor/metal. Strong optical absorption in an ultrathin semiconductor layer is achieved that is robust to variations in the incident angle and polarization state. The modal analysis reveals that this is related to the excitation of a Brewster mode supported by the system that features a flat-band dispersion relation. By examining the reflection phase pickup at the interface between the semiconductor layer and the metal substrate, the physical origin of the strong absorption in the ultrathin layer is discussed. Theoretical studies on the relationship between the incident power flux and the absorption rate reveal that those distinguished physical phenomena occur due to the presence of the highly lossy film that has an imaginary part of the refractive index larger than 0.64. We also present remarks on the feasibility of its application to practical devices such as photodetectors or solar cells with performance estimates.

ACHIEVING OMNIDIRECTIONAL NEAR-UNITY ABSORPTION

Figure 1a shows a schematic diagram of a three-layer configuration composed of a Ge layer sandwiched between free space and a Ag substrate. We plot in Figure 1b the absorption spectrum calculated by the transfer matrix method.[10] The structure is illuminated by a monochromatic plane wave at normal incidence from free space. At a wavelength of 625 nm, near-unity absorption is observed (dotted blue line). It is noteworthy that the fractional absorption in the Ge layer exceeds 98% at this wavelength and remains above around 75% over the visible regime (solid black line). Since the portion of energy absorbed in the Ge layer is dominant, the Ge absorption spectrum (solid black line) and the (Ge + Ag) absorption spectrum (dotted blue line) are hardly distinguished. We can observe a slight discrepancy between them from the inset in Figure 1b.

This high absorption in the Ge layer cannot solely be attributed to the large, intrinsic material absorption. To check the contribution of the material absorption, we plot the single-pass absorption (dash-dotted green line), defined as $A_{SP} = 1 - \exp(-\alpha d)$ (α: attenuation coefficient of Ge; d: Ge thickness). Note that the single-pass absorption itself does not reach 20% at a wavelength of 625 nm. Therefore, it is clear that such a high absorption in the Ge layer is related to the presence of the metal substrate.

It is of interest to compare the strength of the absorption to the well-known Yablonovich limit for broadband light absorption in solar cells derived from thermodynamic principles: $A_Y = 4n^2\alpha d/(1 + 4n^2\alpha d)$.[11−13] For normal incidence, the absorption in the Ge layer exceeds this limit (dashed red line in Figure 1b) at a wavelength of 625 nm. This result does not mean that the absorption enhancement in our config-

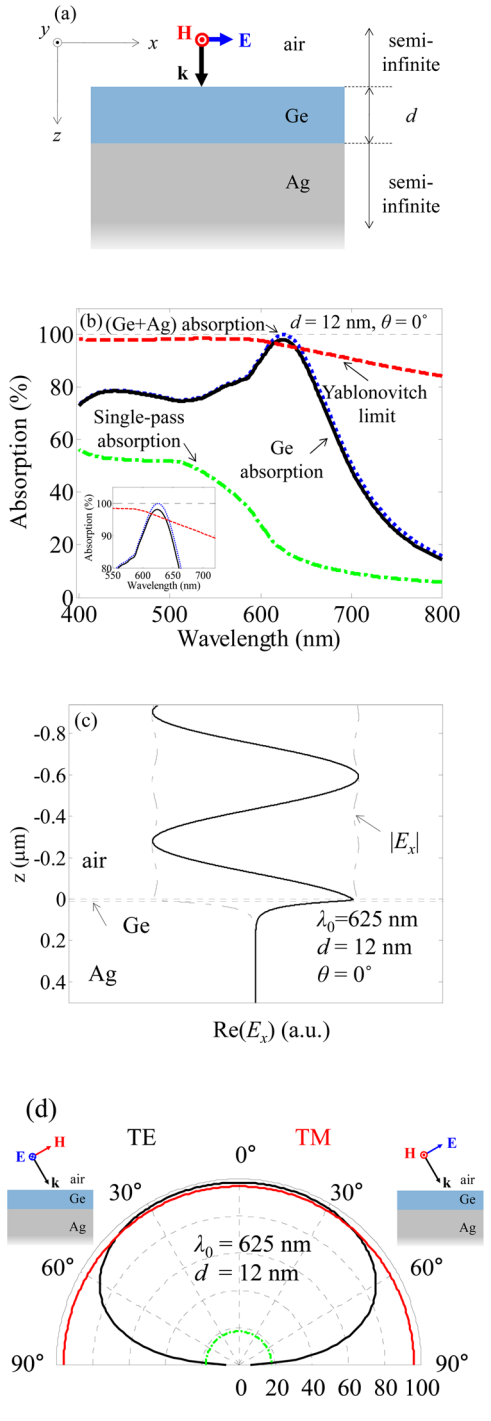

Figure 1. (a) Schematic diagram of air/Ge(12 nm)/Ag Gires-Tournois interferometer. (b) Absorption spectrum for the normal incidence. Dashed red line: Yablonovitch limit; dotted blue line: absorption in Ge (semiconductor) and Ag (metal); solid black line: absorption in Ge; and dash-dotted green line: single-pass absorption. (c) Transverse electric field (x-component) distribution for the air/Ge(12 nm)/Ag case with $\lambda_0 = 625$ nm. Solid line: Re(E_x); dash-dotted line: $|E_x|$. (d) Angle dependence of the absorption at a wavelength of 625 nm and a thickness of 12 nm with the insets depicting the electromagnetic fields for the transverse electric and magnetic polarizations. Solid red line: Yablonovitch limit; dotted blue line: absorption in the semiconductor and metal; solid black line: absorption in the semiconductor; and dash-dotted green line: single-pass absorption.

dx.doi.org/10.1021/ph500093d | ACS Photonics 2014, 1, 812−821

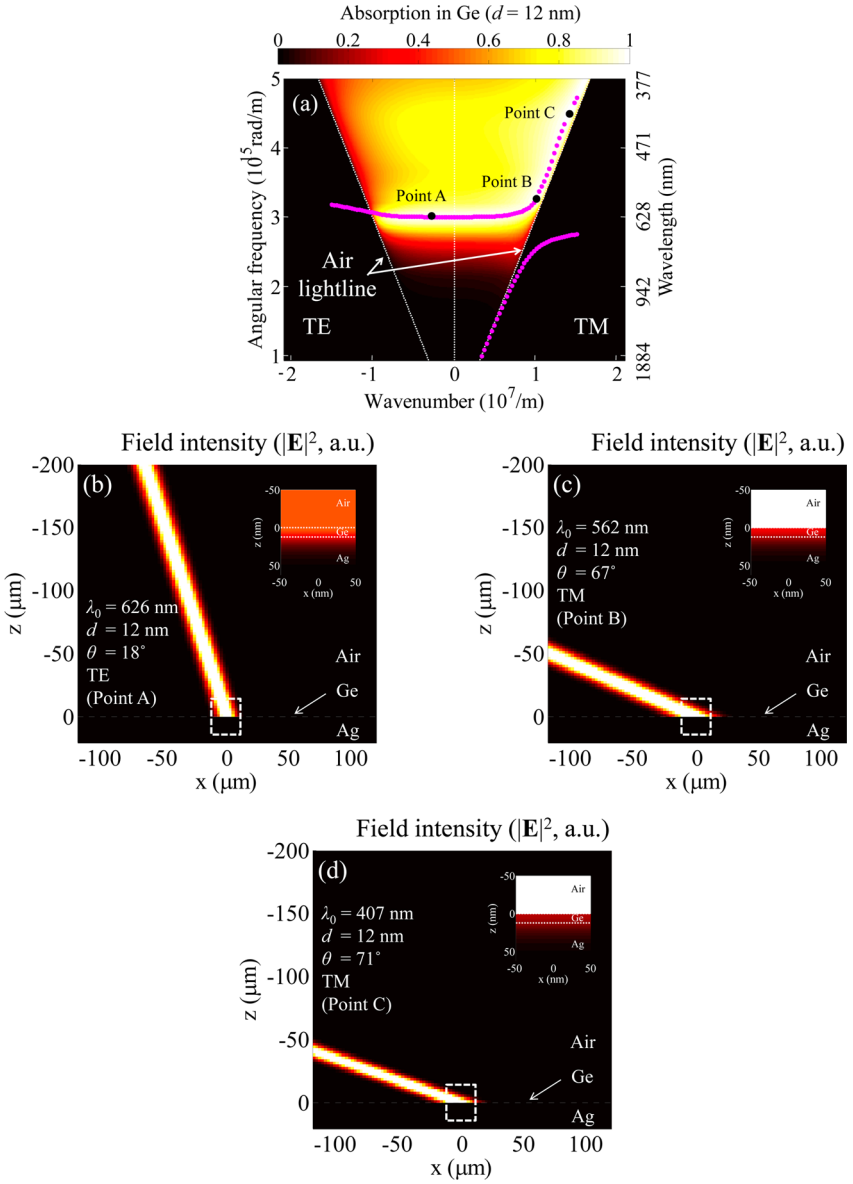

Figure 2. (a) Absorption in the Ge (12 nm) layer (in the color map) with the mode dispersion (in the solid magneta line). The right panel is for the TM case and the left panel the TE case. (b, c, d) Electric field intensity ($|\mathbf{E}|^2$) distributions for the critical coupling points A, B, C in (a), respectively, with the insets depicting the magnified field distribution (the regions denoted by the dashed white lines at the origin).

uration violates this classical limit, which applies only to the weak absorption regime of αd around or below 0.02. Our configuration is in the strong absorption regime with αd around 0.2.[13] To the best of our knowledge, there has not been any theoretical study of the absorption limit in this strong absorption regime.

Figure 1c illustrates the field profile at a wavelength of 625 nm and a Ge thickness of 12 nm. The dash-dotted line indicates the x-component amplitude of the electric field. We see subtle fluctuations in the incident region, which originate from the interference between the incoming electromagnetic wave and the reflected wave; the reflection coefficient R is 0.063%, and the standing wave ratio, defined by $S = (1 + R)/(1 - R)$, is given by 1.0013. For a real metal such as Ag, the field can be seen to penetrate into the metal and the associated energy storage in the metal gives rise to a reflection phase that is larger than that from a perfect electrical conductor (PEC) that does not allow for any field penetration. It will be explained how this reflection phase plays a critical role in affording near-unity, omnidirectional absorption in ultrathin semiconductor films. It is worth pointing out that there is no resonant enhancement of the field with respect to the incident field. In high-quality-factor resonators there is a trade-off between the field enhancement and the operational bandwidth. With the very strong absorption properties of Ge there is no need for a high Q resonance to boost the field and to obtain near-unity absorption. As such, the absorption enhancement can thus be quite broadband.

In analyzing the absorption strength and making a comparison to the absorption limit mentioned above, it is also important to quantify the angular dependence of the absorption. For the derivation of the classic absorption limit it was assumed that the cell is a Lambertian emitter, i.e., it features a very broad angular response. Figure 1d shows the absorption in the Ge layer as a function of the incident angle for the transverse magnetic (TM) and transverse electric (TE) cases, along with the insets depicting the electromagnetic fields and

dx.doi.org/10.1021/ph500093d | ACS Photonics 2014, 1, 812−821

the propagation direction. The wavelength and the Ge thickness are 625 and 12 nm, respectively. The absorption exceeds 80% over incident angles up to 66° and 67° for TM and TE polarizations, respectively. Our configuration exhibits close to omnidirectional absorption properties, and the absorption is robust to changes in the incident angle and the polarization state of the incident light.

To quantitatively assess the performance of this configuration for solar applications, the short-circuit photocurrent density J_{SC} (mA/cm^2) can be estimated assuming 100% internal quantum efficiency.[14]

$$J_{SC} = q \int_{\lambda_B}^{\lambda_G} \alpha(\lambda)\, \Phi_{AM1.5}(\lambda)\, d\lambda \quad (1)$$

Here, q is the charge of the electron (Coulomb), $\alpha(\lambda)$ the absorption coefficient in the Ge layer, and $\Phi_{AM1.5}(\lambda)$ the spectral photon flux density (1/(cm^2·s·nm)) at AM 1.5.[15] λ_G is the band-gap wavelength of Ge (E_G/hc = 1.55 μm with the Ge direct band gap E_G = 0.8 eV, Planck's constant h, and light velocity c), and λ_B is set to 310 nm, considering the high glass absorption below 310 nm. Here we assume the ideal case with the internal quantum efficiency of 100% and normal incidence of light.[16,17] The absorption spectrum shown in Figure 1b results in the short-circuit photocurrent density of 20.0 mA/cm^2.

The suppressed reflection from the proposed configuration is reminiscent of the absorbing antireflection coating (ARC). The ideal ARC shows zero reflection over a wide range of incident angles with broadband operation and robustness to the polarization. There have been a number of diverse ARCs due to their critical importance in various fields such as solar cells, displays, optical elements, and other applications.[18−20] The geometries of ARCs usually include multiple layers of dielectric films or an array of plasmonic metal particles surrounded by dielectric media for index matching. However, there are few ARCs that utilize ultrathin and highly lossy semiconductors as devised in this paper. It is noteworthy that such a simple configuration without any patterning can achieve extreme light absorption over a wide range of incident angles for both polarizations. It will also be shown below that the proposed configuration exhibits broadband absorption.

MODAL ANALYSIS AND CRITICAL COUPLING POINTS

To gain insight into the origin of the omnidirectional, near-unity absorption, we examine the relationship between the spectral absorption and the modal dispersion properties of the system under study. From coupled mode theory we know that the absorption of a planar system under illumination reaches a maximum when the energy and momentum of the incident light are matched to a supported mode in the system. For example, the fact that a metal/air interface supports a surface plasmon polariton (SPP) mode results in a dip in the angular reflection spectrum in a prism coupling experiment.[21] On the basis of our observation of strong absorption, it hence is expected that our configuration—air/thin semiconductor film/metal substrate—would support a certain mode supported along the semiconductor film. With an understanding of the nature of this mode, it should become possible to judiciously engineer the absorption strength and spectral properties.

First, we calculate the absorption in the 12 nm thick Ge layer on top of the Ag substrate as a function of the angular frequency ranging from 1×10^{15} to 5×10^{15} rad/s and incident angles from 0° to 90° for both TM and TE polarization (see Figure 2a). These calculations were performed using the transfer matrix method.[10] The strength of the absorption for these polarization states is plotted in a dispersion diagram (energy vs the magnitude of the in-plane wavenumber k) in anticipation that the absorption feature can be closely linked to the dispersion relations of the modes supported by the system. As the absorption features for both polarizations are symmetric around k = 0, we have plotted the absorption in the 2-D color map for TM polarization in the positive k-direction and TE polarization in the negative k-direction. Note that the system exhibits a maximum in the absorption around a wavelength of 625 nm and the absorption is quite robust to variations in the wavenumber, as shown above. Strong absorption for grazing incidence illumination in the TM case is also observed. This can be ascribed to the Brewster angle, at which the wave impedance of the Ge film is matched to that of air and the reflection at the air/Ge interface is negligible.

Next, the supported modes of our configuration are analyzed. In our experiment, we illuminate the layered system with a beam of light at a well-defined incident angle. This imposes a real-valued wavenumber on the modes that can be excited in the system. For this reason, we will analyze the possible excitation of Brewster modes,[21,22] which feature a well-defined, real-valued wavenumber and a complex-valued angular frequency. It is worth pointing out that the Brewster mode is physically distinct from a leaky mode; the Brewster mode, or the surface mode, refers to a mode with an incoming energy flow from the semi-infinite open-cladding (air, in our case) to the system, whereas the leaky mode, or the virtual mode, corresponds to a mode with an outgoing energy flow from the system to the semi-infinite open-cladding.[21,22] In studying Brewster modes, one is interested in assessing the lifetime of a mode using a complex frequency analysis as opposed to a study of leaky modes, where one is interested in assessing the propagation length in the complex wavenumber domain. By allowing all possible cases in the characteristic equation,[23] we can obtain a continuous modal dispersion curve.

In comparing the transfer matrix calculations of the absorption to the results from the modal analysis, we see that the regions of maximum absorption perfectly coincide with the mode dispersion curve. This agreement indicates that the absorption maximum occurs when the incident light can excite the supported Brewster mode. When we chose the leaky mode instead of the Brewster mode, we observed a discrepancy between the dispersion relation of the leaky mode and the maximum absorption conditions (not shown here). Considering that there has been considerable research that interprets the absorption phenomenon as the coupling from the radiation (incident) mode to the leaky mode supported by the system, our result raises a notable issue. We think apparent good agreements that have been observed so far in other configurations with small material losses may originate from the degenerate dispersion relation between the Brewster mode and the leaky mode. As the material loss becomes larger, the dispersion relations of the Brewster mode and the leaky mode get separated and the maximum absorption condition coincides with the dispersion relation of the Brewster mode, rather than that of the leaky mode.

The second observation is that our configuration exhibits a quasi flat-band mode dispersion (see the solid magenta line in Figure 2a). This indicates that the Brewster mode supported in

dx.doi.org/10.1021/ph500093d | ACS Photonics 2014, 1, 812−821

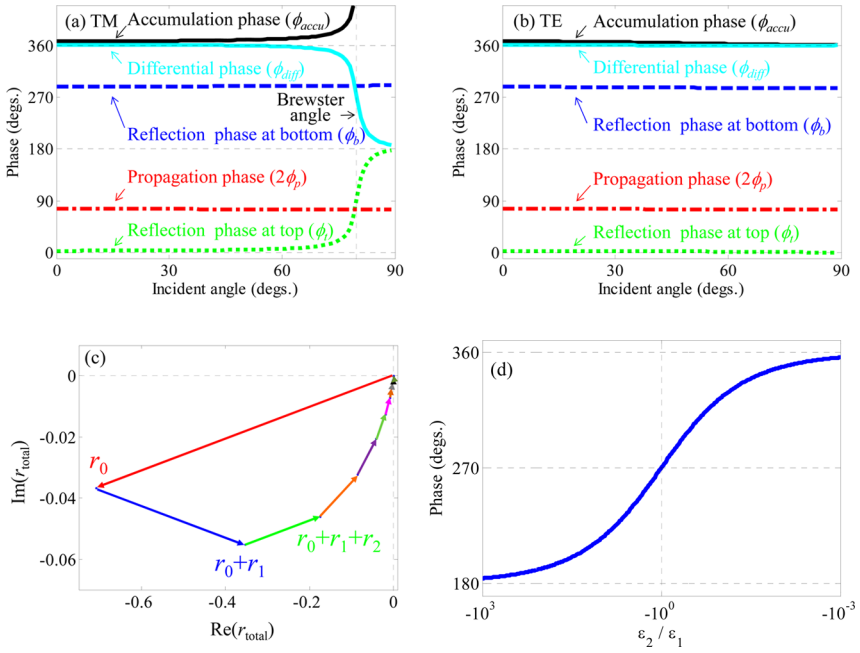

Figure 3. (a) Reflection and propagation phases as a function of the incident angle at a wavelength of 625 nm and a Ge thickness of 12 nm. Dash-dotted red line: propagation phase retardation in the semiconductor; dotted green line: reflection phase pickup at the top interface (air/Ge); solid black line: total phase; and dashed blue line: reflection phase pickup at the bottom (Ge/Ag). (b) TE result. The line legends are the same as in (a). (c) Trajectory of sums of the partial reflected waves at the critical coupling condition: point A in Figure 2a. (d) Reflection phase from a layer with ε_1 to a layer with $\varepsilon_2 = \varepsilon_{2,r} + i\varepsilon_{2,i}$ where $\varepsilon_{2,r} < 0$ and $\varepsilon_{2,i} = 0$ as a function of $\varepsilon_2/\varepsilon_1$.

our configuration can take on a wide variety of wave numbers at one operating frequency. As a result, plane waves with a wide range of incident angles can be coupled to the mode supported in the system, leading to omnidirectional absorption. Such a flat-band dispersion is reminiscent of the omnidirectional resonance presented in a previous work on planar metal−insulator−metal cavities.[6] In the previous case, the flat-band dispersion originates from compensation between the propagation and reflection phases. As the incident angle increases, the propagation phase decreases, whereas the reflection phase increases. This phase compensation occurs only for the TM case in the previous system.[6] In contrast, the system presented here exhibits this behavior for the TE illumination also. This gives rise to near-unity, broad-angle, and polarization-independent light absorption properties.

The third remark in the modal analysis is that this modal dispersion is a line connecting several critical coupling points and the absorption remains near-unity along this line. As can be seen in Figure 2a, the critical coupling points are located at (ω, $k_{\|}$) = (3.01×10^{15} rad/s, 0.316×10^7/m)—(λ_0, θ) = (626 nm, 18°)—for the TE case (point A in Figure 2a) and (ω, $k_{\|}$) = (3.35×10^{15} rad/s, 1.03×10^7/m)—(λ_0, θ) = (562 nm, 67°)—and (4.62×10^{15} rad/s, 1.46×10^7/m)—(λ_0, θ) = (407 nm, 71°)—for the TM case (points B and C in Figure 2a, respectively), where $k_{\|}$ and θ denote the in-plane (x-axis) wavenumber and the incident angle, respectively. At these points, the incoming photon flux to the system exactly equals the dissipation rate, and thus the reflection is zero and the absorption in Ge and Ag has to reach a unity value.[24] Figures 2b−d show the electric field intensity ($|E|^2$) distributions at the critical coupling points A, B, and C in Figure 2a, respectively, under Gaussian beam illumination with a beam width of $10\lambda_0$. The insets in Figure 2b−d show the magnified field distribution at the origin denoted by the dashed white box. We note that at those critical coupling points the reflections are almost zero, and there is little oscillation in the field distribution above the sample due to the formation of a standing wave. Intriguingly, we still observe near-unity absorption away from these critical points. Along the modal dispersion line connecting the critical coupling points, the absorption remains above 96%. This phenomenon can also be applied to other material combinations beyond Ge and Ag. In other words, by engineering mode dispersions in such a way that they connect several critical coupling points, we can achieve omnidirectional and polarization-independent near-unity absorption in various material combinations such as germanium and gold, or amorphous silicon and silver. This will be discussed in more detail below. This anomalous behavior has also been reported in complete optical tunneling.[25−27] In ref 27, two complete tunneling conditions closely located to each other result in a flat-top unity transmission for a certain range of wavelengths or incident angles. This general phenomenon may prove a promising direction for future investigation in many optics-related fields.

ROLE OF REFLECTION PHASE IN REACHING NEAR-UNITY ABSORPTION

When optimizing light−matter interaction in planar, translationally invariant systems, one typically thinks of driving a Fabry−Pérot resonance. The resonance condition for this type of resonance is that the total phase accumulation upon one round-trip in the cavity should equal an integer multiple of 2π ($2m\pi$, m = 1, 2, 3, ...). For ultrathin devices, we consider the case for which m = 1. Our system with a thin film deposited on a metallic backreflector, on the contrary, is a Gires−Tournois style interferometer.[28] This style interferometer typically features a transparent dielectric film, and this type of reflector stack provides a unique spectral dependence of the group delay that can be used for pulse compression.[29] In this work, we

dx.doi.org/10.1021/ph500093d | ACS Photonics 2014, 1, 812−821

consider a strongly absorbing semiconductor film and aim to optimize the absorption in this layer.

Figures 3a and b show the phase for the TM and TE cases, respectively. Dash-dotted red curves denote the propagation phase pickup ($2\phi_p$) in the Ge layer, dashed blue curves the reflection phase pickup at the bottom boundary (ϕ_b, from Ge to Ag layer), and dotted green curves the reflection phase pickup at the top boundary (ϕ_t, from Ge layer to air). It appears the accumulation phase ($\phi_{accu} = 2\phi_p + \phi_b + \phi_t$, depicted by the solid black curve) displays near 2π (or 360°). However, a closer look reveals that the accumulation phase that maximizes the absorption is different from 2π. Rather, the differential phase, which is defined as

$$\phi_{diff} = 2\phi_p + \phi_b - \phi_t \quad (2)$$

(depicted by the solid cyan curve), displays the exact 2π at the angle of the critical coupling condition. This is a unique feature of a Gires–Tournois resonator, which is distinct from a Fabry–Pérot resonator, which requires an accumulation phase of 2π.

This conundrum has been raised by Kats, Capasso, and their colleagues[8,30] and can be understood by investigating the condition of partial reflected waves for the destructive interference in the Gires–Tournois configuration. Figure 3c shows a trajectory of the partial sum of the reflected waves. Here r_0 is the complex reflection amplitude of the directly reflected wave from air to the Ge layer, r_1 the partial reflected wave that undergoes one round-trip in the Ge layer, and r_n the partial reflected wave that has made n round-trips. Owing to the strong loss in the Ge layer, the phase of r_0 is not π; instead, it displays a complex phase. As a result, the partial reflected waves do not need to be aligned, having the same phase, and ϕ_{accu} can be different from $2m\pi$. In addition, the condition of $\phi_{diff} = 2m\pi$ can be derived from the Airy formula:[8,31]

$$r_{total} = \frac{r_{12} - r_{23}e^{2i\beta d}}{1 - r_{12}r_{23}e^{2i\beta d}} \quad (3)$$

where r_{12} is the reflection from air to the Ge layer, r_{23} is the reflection from Ge to Ag, β is the longitudinal wavenumber in the Ge layer, and d is the thickness of the Ge layer. The unity absorption condition is met when the numerator of eq 3 vanishes; $r_{12} - r_{23}\exp(2i\beta d) = 0$. The phase relationship for this condition is summarized as $\phi_{diff} = 2m\pi$. Note that, in the absence of the loss, ϕ_t is zero, which indicates that the plus and minus signs for ϕ_t cannot be distinguished. Therefore, ϕ_{accu} becomes the same as ϕ_{diff}.

Each phase term remains almost constant for the wide range of incident angles. This is because the discrepancy between the indices of free space and the Ge layer is significant, and thus, according to Snell's law, the refraction angle in the Ge layer remains very small over a wide range of incidence angles in free space. As a result, the amplitude change of the longitudinal wavenumber (in the z-direction) in the Ge layer is almost zero, leading to a negligible change of phase accumulation during reflection and propagation upon the incident angle change.

The TM case has a unique transition point where the reflection phase changes at the top interface from zero to π. This point corresponds to the Brewster angle θ_B, at which TM-polarized light is perfectly transmitted (without reflection) from the air into the Ge layer. The magnitude of this angle is determined by the ratio of the refractive indices of the incident medium (air in our case) n_i and the medium that the light transmits into n_t (Ge in our case): $\theta_B = \arctan(n_t/n_i)$. If the index difference between two media is not significant, the presence of the Brewster angle in the TM case would introduce a strong dependence on the incidence angle. However, given the high index of the Ge layer, the Brewster angle is pushed out to about 80° and the presence of the Brewster angle does not have a significant effect on the angular dependence of the light absorption.

So far, we have discussed two distinct absorption properties of the semiconductor-on-metal configuration: near-unity absorption and omnidirectionality; however, the reported absorption is also significant given the extremely small thickness of the Ge layer. For example, the 12 nm thick Ge layer can absorb more than 98% of the light energy at a wavelength of 625 nm at normal incidence. We will argue that to achieve near-unity absorption, one needs to both satisfy a destructive interference condition in the Gires–Tournois configuration and have a semiconductor layer with very strong absorption, i.e., a high imaginary part of the dielectric constant. The Gires–Tournois interference would require a thickness around $\lambda_0/4n_s$, where n_s is the real part of the refractive index of the semiconductor layer ($n_s = 5.5$ at $\lambda_0 = 625$ nm for Ge).[5,6] It turns out that the near-unity absorption is enabled by the reflection phase pickup from the semiconductor to the metal substrate. This can be seen by analyzing the maximum absorption condition in eq 2 for a semiconductor film exhibiting the lowest order interference ($m = 1$) by including the phase pickups that can occur and the top and bottom interfaces: $\phi_{diff} = 2\phi_p + \phi_b - \phi_t = 2n_sk_0d + \phi_b - \phi_t = 2\pi$. Even for strong semiconductors, ϕ_t tends to be small (typically less than 10°) compared to the other propagation phase and reflection phase at the bottom reflector. For this reason, we ignore this phase in the argument below. If the perfect electric conductor is adopted as the substrate, the electric field cannot penetrate into the substrate and vanishes at the interface. This results in a reflection phase $\phi_{b,PEC}$ of π, leading to a condition where $d = \lambda_0/4n_s$ in order to maximize absorption. If we use metals with finite dielectric constants, the electric field has a nonvanishing penetration into the deep metal substrate (see the field distribution presented in Figure 1c). Consequently, the reflection phase pickup becomes larger and the required semiconductor thickness is smaller. The reflection phase pickup from a semiconductor layer to a metal with finite conductivity depends on the ratio between the amplitudes of dielectric constants in the semiconductor and metal. Figure 3d shows the reflection phase pickup from a layer with ε_1 to a hypothetical lossless metal with $\varepsilon_2 = \varepsilon_{2,r} + i\varepsilon_{2,i}$ where $\varepsilon_{2,r} < 0$ and $\varepsilon_{2,i} = 0$ as a function of $\varepsilon_2/\varepsilon_1$. As the metal has smaller $|\varepsilon_2|$, the reflection phase pickup increases from π (or 180°) to 2π (or 360°).

One can make a quick intuitive estimate of the magnitude of the imaginary part of the refractive index that is required to produce the maximum absorption. With the absorbed power per unit volume equaling $Q_{Abs} = 0.5\omega\varepsilon_0\ \mathrm{Im}(\varepsilon)|E|^2$ and the incident power equaling $P_{Inc} = 0.5c\varepsilon_0|E_0|^2$ the absorptance is

$$A = \int dQ_{Abs}/P_{Inc} = k_0\ \mathrm{Im}(\varepsilon)\left(\int |E(z)|^2 dz\right)/|E_0|^2 \quad (4)$$

Here, $|E_0|$ is the magnitude of the incident light wave and $|E|$ is the magnitude of the electric field in the film. On resonance with a perfect electric conductor, the electric field intensity is around $|E_0|^2$ at the surface and zero at the conductor surface. Therefore, we can estimate $\int |E|^2\, dz$ in eq 4 to be roughly equal to $(d/2)|E_0|^2$. By putting this result into eq 4 as well as unity absorption ($A = 1$), we have $k_0(d/2)\ \mathrm{Im}(\varepsilon) = n_Sk_Sk_0d \approx 1$,

dx.doi.org/10.1021/ph500093d | ACS Photonics 2014, 1, 812–821

where k_S is the imaginary part of the refractive index of the semiconductor layer. Here the product $n_S k_0 d$ is fixed by the maximum absorption conditions expressed in eq 2. With the reflection phase at Ge/Air being small, the maximum absorption condition can be rewritten as $n_S k_0 d \approx \pi - \phi_b/2$. We thus find that $k_S \approx 1/(\pi - \phi_b/2)$. For a PEC ($\phi_b = \pi$) we find $k_S \approx 2/\pi \approx 0.64$. For a "softer" metal that allows for field penetration with $|\varepsilon_s| \approx |\varepsilon_m|$ and a reflection phase $\phi_b = 1.5\pi$, $k_S \approx 4/\pi \approx 1.27$. For most common metals the required k_S for the semiconductor layer will lie between these values.

The wavelength of maximum absorption can be easily tuned by changing the semiconductor layer thickness. Figure 4a shows the absorption spectra (solid lines) and the classical limits (dashed lines) for the Ge layer thickness of 10 nm (red), 20 nm (green), and 30 nm (blue), respectively. The absorption peak wavelength red-shifts with increasing film thickness as a longer wavelength requires a thicker cavity to stay on resonance. As the Ge layer gets thicker, the absorption peak exhibits a red-shift and is reduced in magnitude, falling below the Yablonovitch limit. This is because the imaginary part of the dielectric constant of Ge in this spectral range is not sufficiently high. In order to quantitatively analyze the extent of the red-shift, we plot in Figure 4b the absorption peak wavelength as a function of the Ge layer thickness. The slope is obtained to be around 12.5. This indicates the slight change of the Ge thickness on the order of tens of nanometers can give rise to a substantial shift of the resonance wavelength on the order of hundreds of nanometers, allowing for manipulation of the absorption band.

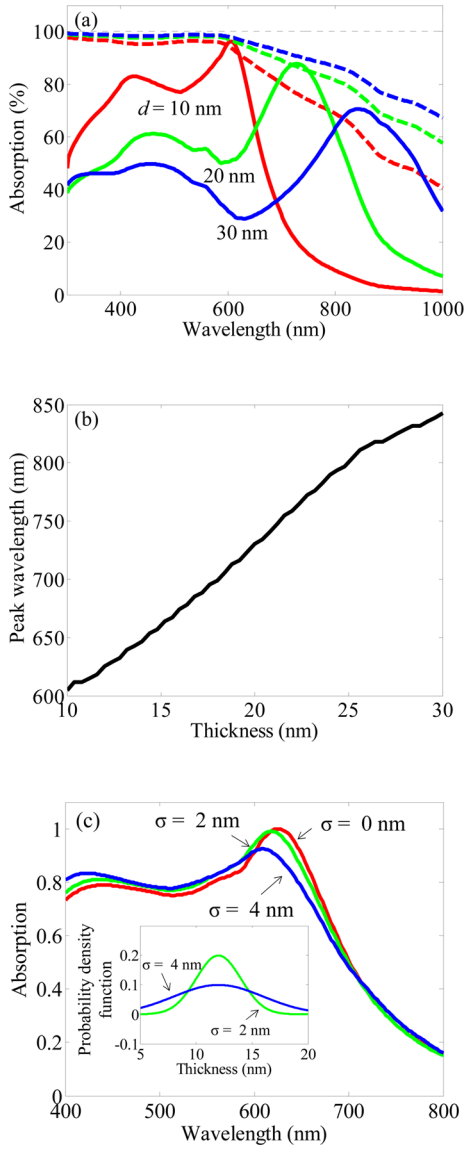

Figure 4. (a) Absorption spectrum (solid line) and Yablonovitch limit (dashed line) for the air/Ge/Ag configuration with a Ge thickness of 10 nm (red), 20 nm (green), and 30 nm (blue). (b) Absorption peak wavelength as a function of the semiconductor thickness. (c) Absorption spectrum for the air/Ge/Ag configuration with the normal distribution (shown as the inset) of the Ge thickness. The standard deviation (σ) is 0 nm (red), 2 nm (green), and 4 nm (blue), and the mean is 12 nm.

So far we have assumed the ideal case of perfectly planar films with uniform thickness. Practical devices may have nonuniform film thickness. To investigate the effect of such a nonideal case, we carried out calculations of the absorption spectrum in the air/Ge/Ag Gires–Tournois interferometers. The thickness is assumed to exhibit a normal distribution with a mean thickness of 12 nm, which is the same as that used in the ideal case, and various standard deviations (σ). The absorption spectra for a σ of 0 nm (the ideal case), 2 nm, and 4 nm and the thickness distributions are shown in Figure 4c and its inset with the red, green, and blue lines, respectively. The slight discrepancy from the ideal case is observed for the absorption spectrum for the standard deviation of 2 nm (green), indicating that the proposed configuration is robust to thickness nonuniformity. As we increase the thickness deviation up to 4 nm (blue), the maximum absorption peak gets weaker The absorption in the short-wavelength range grows slightly. This can be ascribed to the presence of thin Ge layers. As a result of an averaging effect, the short-circuit photocurrent densities are 20 mA/cm^2 for the thickness standard deviations of 0, 2, and 4 nm.

DESIGN RULES AND APPLICATIONS

We can extend our analysis to more generalized design rules by exploring several combination materials systems widely used in energy-harvesting applications, such as germanium, amorphous silicon (a-Si), gallium arsenide, and copper indium gallium selenide (CIGS), whose refractive indices are presented in the top panel of Figure 5, with diverse metal substrates including silver, gold, and aluminum, whose dielectric constants are shown in the left panel of Figure 5.

Let us first examine the second upper panel (with Ag substrate). Ge, a-Si, GaAs, and CIGS can be designed to display strong light absorption, in excess of 95%, over the wavelength regions of 600–648, 480–576, 432–462, and 300–498 nm, respectively, by changing the thickness. As expected, this regime corresponds in each materials system to a wavelength range in which the imaginary part of the material index (k_S) is around 0.64–1.27. Ge and CIGS feature a wider range of high absorption, and this can be ascribed to their material properties of moderate material loss (k_S of 0.64–1.27) over a broad spectral range. Another remark is that there is a limit to the tunability of the high-absorption wavelength (absorption above 95% in the semiconductor) with thickness in the air/semiconductor/metal configuration. It was pointed out above that the maximum absorption is achieved whenever the maximum absorption condition is met, and the thickness can be chosen in such a way that the differential phase is equal to an

dx.doi.org/10.1021/ph500093d | ACS Photonics 2014, 1, 812–821

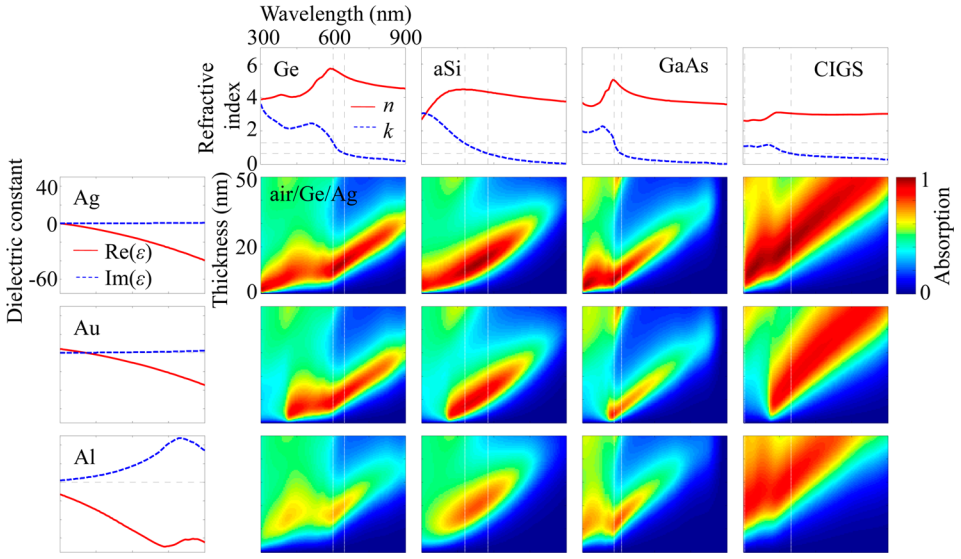

Figure 5. Absorption spectrum for various material combinations with semiconductors (Ge, a-Si, GaAs, and CIGS) and metal substrates (Ag, Au, and Al). The bands with $0.64 < k < 1.27$ are indicated by dashed black lines in the optical properties of semiconductors under consideration (upper panels) and dashed white lines in the resultant absorption maps.

integer multiple of 2π at a given wavelength. Therefore, we can say that the fundamental design parameter is the thickness of the semiconductor. The general design rule is to set the thickness so as to satisfy the zero-differential phase defined in eq 2. By changing the thickness of the semiconductor, the propagation phase ϕ_p can be tuned. It is also noteworthy that, even though the resonant wavelength itself can be tuned by changing the semiconductor thickness, the significant absorption is also related to the material properties. From this perspective CIGS offers the most attractive performance.

If one is seeking a material combination for a broadband application rather than efficient absorption at a specific operating wavelength, an additional constraint is imposed. We have demonstrated that substantial absorption in the active layer is achieved in a given material when the imaginary part of the refractive index (k_S) is in the range 0.64−1.27. Broadband operation requires that the maximum absorption condition is satisfied over a broad wavelength range. Given that in most cases the round-trip phase exhibits the strongest wavelength dependence, it is important to keep nk_0 close to constant. This can be attained only in spectral regions where a semiconductor features abnormal dispersion, i.e., where the real part of the refractive index n decreases with increasing wavelength. It is noteworthy that Ge does exhibits such abnormal dispersion for wavelengths of 470−600 nm. A metamaterial with a linearly increasing n_S and a constant k_S around 0.64−1.27 could perhaps be designed by means of a smart mixing strategy of Ge and other materials with smaller k_S.

Important remarks can also be given regarding the choice of the metal substrate. We observe that the noble metals, Ag and Au, always beat other metals such as Al. This is directly related to high material loss in Al. In the same context, Ag is superior to Au; the Ag case always shows stronger absorption in the semiconductor. In addition, 410 nm is the plasma wavelength of Au, below which a Au substrate becomes transparent and no longer acts as a good reflector. As a result, films on a Au substrate have an abrupt decrease in absorption for wavelengths below 410 nm.

Meanwhile, materials such as quantum dots and organics are not highly lossy, and their imaginary parts of the refractive index are much smaller than 0.64. The way these fields can benefit from the proposed architecture is to design and implement a metamaterial/metasurface composed of low-loss and high-loss material. Under appropriate modelings such as the Maxwell−Garnett formula, the overall optical response of such metamaterials can be described by an arithmetic or harmonic mean of the dielectric functions of two materials consisting of the metamaterial, and it is possible to obtain enhanced material absorption. As we plug in our proposed theory to those metamaterials with higher loss, it is expected that significantly efficient optical absorption could be achieved.

The devised configuration has various potential applications such as photodetectors and solar cells, in which the absorbed photon energy is used to generate electron−hole pairs. We note that the bottom metal substrate can be used as an electrical contact for charge extraction as well as a reflector. In order to extract the other charge carrier, a transparent conducting oxide such as indium−tin-oxide (ITO) can be deposited on top of the semiconductor, as shown in the inset of Figure 6a. The presence of this additional layer would affect the absorption characteristics. However, significant absorption can still be realized. Figure 6a shows the absorption spectrum for various thickness combinations of ITO (d_{ITO}) and Ge (d_{Ge}). Substantially enhanced absorption over the visible spectral region is observed when d_{ITO} = 15 nm and d_{Ge} = 8 nm. The calculation for eq 1 reveals that the maximum short-circuit photocurrent density available in our configuration is around 17.5 mA/cm^2 (d_{ITO} = 15 nm and d_{Ge} = 8 nm). It is remarkable that a mere 8 nm thick semiconductor can be used to generate this level of the short-circuit photocurrent density, although this value is less than the short-circuit photocurrent density 20.0 mA/cm^2 for the case of the 12 nm thick Ge layer without the ITO layer. To circumvent this reduction in the short-circuit photocurrent density due the presence of the additional ITO layer, one may implement an absorber with separated backside electron and hole contacts for p- and n-doped Ge, as shown in

dx.doi.org/10.1021/ph500093d | ACS Photonics 2014, 1, 812−821

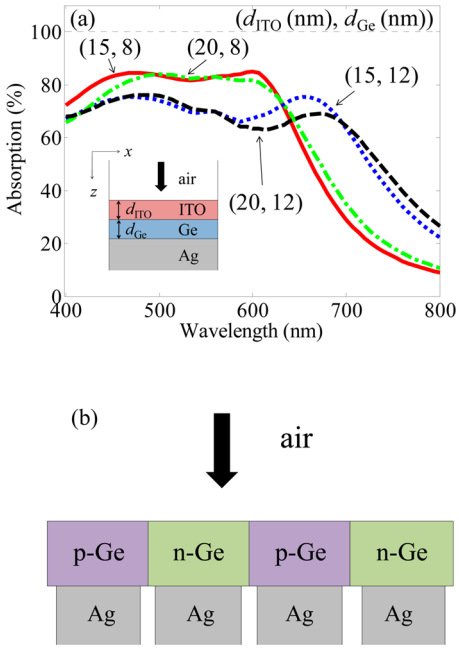

Figure 6. (a) Absorption spectrum for air/ITO/Ge/Ag for various thickness combinations of d_{ITO} and d_{Ge} in nm. Solid red: 15 nm, 8 nm; dotted blue: 15 nm, 12 nm; dash-dotted green: 20 nm, 8 nm; and dashed black: 20 nm, 12 nm. (b) Schematic of solar cells based on the separate electron and hole contacts for p- and n-doped Ge.

Figure 6b, in which the generated carriers are extracted to isolated, laterally placed Ag contacts.[32]

CONCLUSION

We presented a near-unity omnidirectional optical absorption mechanism for an ultrathin semiconductor layer on top of a judiciously chosen metal substrate. Significant absorption in the ultrathin active semiconductor layer up to 98% is demonstrated with a remarkable omnidirectional response. The physical origin of these phenomenal features is understood by rigorous investigations of the flat-band Brewster mode that connects the three critical coupling points supported in the system. This flat-band property is elucidated by means of the reflection and propagation phase relationships. The devised configuration and physical insight may shine light on the development of highly efficient, ultrathin photodetectors and solar cells.

AUTHOR INFORMATION

Corresponding Author

*E-mail: brongersma@stanford.edu.

Notes

The authors declare no competing financial interest.

ACKNOWLEDGMENTS

This work was supported by the Precourt seed grant project on ultrathin light absorbers for solar cells and a National Research Foundation of Korea (NRF) grant funded by the Korean government (MEST) (2013R1A6A3A03060952). We appreciate fruitful discussions with and valuable comments by Soo Jin Kim, Sang Moo Jeong, Hadiseh Alaeian, Toby Sachs-Quintana, Zongfu Yu, Krishna C. Balram, Sander Mann, and Mikhail Kats.

REFERENCES

(1) Teperik, T. V.; García de Abajo, F. J.; Borisov, A. G.; Abdelsalam, M.; Bartlett, P. N.; Sugawara, Y.; Baumberg, J. J. Omnidirectional absorption in nanostructured metal surfaces. *Nat. Photonics* **2008**, *2*, 299−301.

(2) Liu, N.; Mesch, M.; Weiss, T.; Hentschel, M.; Giessen, H. Infrared perfect absorber and its application as plasmonic sensor. *Nano Lett.* **2010**, *10*, 2342−2348.

(3) Wu, C.; Neuner, B., III; Shvets, G.; John, J.; Milder, A.; Zollars, B.; Savoy, S. Large-area wide-angle spectrally selective plasmonic absorber. *Phys. Rev. B* **2011**, *84*, 075102.

(4) Hägglund, C.; Zeltzer, G.; Ruiz, R.; Thomann, I.; Lee, H.-B.-R.; Brongersma, M. L.; Bent, S. F. Self-assembly based plasmonic arrays tuned by atomic layer deposition for extreme visible light absorption. *Nano Lett.* **2013**, *13*, 3352−3357.

(5) Biener, G.; Niv, A.; Kleiner, V.; Hasman, E. Metallic subwavelength structures for a broadband infrared absorption control. *Opt. Lett.* **2007**, *32*, 994−996.

(6) Shin, H.; Yanik, M. F.; Fan, S.; Zia, R.; Brongersma, M. L. Omnidirectional resonance in a metal-dielectric-metal geometry. *Appl. Phys. Lett.* **2004**, *84*, 4421.

(7) Cho, S.-H.; Seo, M.-K.; Kang, J.-H.; Yang, J.-K.; Kang, S.-Y.; Lee, Y.-H.; Hwang, K. H.; Lee, B. D.; Lee, J.-G.; Song, Y.-W.; Lee, J. H. A black metal-dielectric thin film for high-contrast displays. *J. Korean Phys. Soc.* **2009**, *55*, 501−507.

(8) Kats, M. A.; Blanchard, R.; Genevet, P.; Capasso, F. Nanometre optical coatings based on strong interference effects in highly absorbing media. *Nat. Mater.* **2013**, *12*, 20−24.

(9) Dotan, H.; Kfir, O.; Sharlin, E.; Blank, O.; Gross, M.; Dumchin, I.; Ankonina, G.; Rothschild, A. Resonant light trapping in ultrathin films for water splitting. *Nat. Mater.* **2013**, *12*, 158−164.

(10) Saleh, B. E. A.; Teich, M. C. *Fundamentals of Photonics*, 2nd ed.; Wiley Intersceince: Hoboken NJ, 2007.

(11) Yablonovitch, E. Statistical ray optics. *J. Opt. Soc. Am.* **1982**, *72*, 899−907.

(12) Green, M. A. Lambertian light trapping in textured solar cells and light-emitting diodes: analytical solutions. *Prog. Photovolt: Res. Appl.* **2002**, *10*, 235−241.

(13) Yu, Z.; Raman, A.; Fan, S. Thermodynamic upper bound on broadband light coupling with photonic structures. *Phys. Rev. Lett.* **2012**, *109*, 173901.

(14) Hägglund, C.; Apell, S. P. Resource efficient plasmon-based 2D-photovoltaics with reflective support. *Opt. Express* **2010**, *18*, A343−A356.

(15) National Renewable Energy Laboratory. *Reference Solar Spectral Irradiance: Air Mass 1.5*; http://rredc.nrel.gov/solar/spectra/am1.5 (accessed January 20, 2014).

(16) Wang, K. X.; Yu, Z.; Liu, V.; Cui, Y.; Fan, S. Absorption enhancement in ultrathin crystalline silicon solar cells with antireflection and light-trapping nanocone gratings. *Nano Lett.* **2012**, *12*, 1616−1619.

(17) Cao, L.; Fan, P.; Vasudev, A. P.; White, J. S.; Yu, Z.; Cai, W.; Schuller, J. A.; Fan, S.; Brongersma, M. L. Semiconductor nanowire optical antenna solar absorbers. *Nano Lett.* **2010**, *10*, 439−445.

(18) Sun, X.; Chen, X.; Zhang, Z.; Sun, Z. Plasmon based antireflection coatings containing nanostructured Ag and silica medium. *Appl. Surf. Sci.* **2012**, *258*, 3785−3788.

(19) Moiseev, S. G. Composite medium with silver nanoparticles as an anti-reflection optical coating. *Appl. Phys. A: Mater. Sci. Process.* **2011**, *103*, 619−622.

(20) Spinelli, P.; Verschuuren, M. A.; Polman, A. Broadband omnidirectional antireflection coating based on subwavelength surface Mie resonators. *Nat. Commun.* **2011**, *3*, 692.

(21) Ferguson, P.; Wallis, R. F.; Belakhovsky, M.; Jadot, J. P.; Tomkinson. Surface plasma waves in silver and gold. *J. Surf. Sci.* **1978**, *76*, 483−498.

(22) Burstein, E.; Hartstein, A.; Schoenwald, J.; Maradudin, A. A.; Mills, D. L.; Wallis, R. F. Surface polaritons-electromagnetic waves at interfaces. In *Proceedings of the First Taormina Research Conference on*

the Structure of Matter; Burstein, E.; Martine, F. De, Eds.; Pergamon: New York, 1974.
(23) Burke, J. J.; Stegeman, G. I.; Tamir, T. Surface-polariton-like waves guided by thin lossy metal films. *Phys. Rev. B* **1986**, *33*, 5186−5201.
(24) Tischler, J. R.; Bradley, M. S.; Bulović, V. Critically coupled resonators in vertical geometry using a planar mirror and a 5 nm thick absorbing film. *Opt. Lett.* **2006**, *31*, 2045−2047.
(25) Park, J.; Kim, K.-Y.; Lee, B. Complete tunneling of light through a composite barrier consisting of multiple layers. *Phys. Rev. A* **2009**, *79*, 023820.
(26) Kim, K.-Y.; Park, J.; Lee, B. Complete tunneling of normally incident light through singly negative materials. *Phys. Rev. A* **2009**, *79*, 055801.
(27) Kim, K.-Y.; Lee, B. Application of complete tunneling to flat-top total transmission filters. *IEEE Photon. Technol. Lett.* **2008**, *20*, 1057−1059.
(28) Gires, F.; Tournois, P. An interferometer useful for pulse compression of a frequency modulated light pulse. *C. R. Acad. Sci. Paris* **1964**, *258*, 6112−6115.
(29) Li, K. D.; Knox, W. H.; Pearson, N. M. Broadband cubic-phase compensation with resonant Gires-Tournois interferometers. *Opt. Lett.* **1989**, *14*, 450−452.
(30) Kats, M. A.; Sharma, D.; Lin, J.; Genevet, P.; Blanchard, R.; Yang, Z.; Qazilbash, M. M.; Basov, D. N.; Ramanathan, S.; Capasso, F. Ultra-thin perfect absorber employing a tunable phase change material. *Appl. Phys. Lett.* **2012**, *101*, 221101.
(31) Born, M.; Wolf, E. *Principles of Optics*, 7th ed.; Cambridge University Press: Cambridge UK, 1999.
(32) Würfel, P. *Physics of Solar Cells: From Principles to New Concepts*; Wiley-VCH: Weinheim, 2005.